Physica Medica 81 (2021) 197–209

Contents lists available at ScienceDirect

Physica Medica

journal homepage: www.elsevier.com/locate/ejmp

Technical note

Steerable3D: An ImageJ plugin for neurovascular enhancement in 3-D segmentation

Paolo Miocchi [a], Alejandra Sierra [b], Laura Maugeri [a,c], Eleonora Stefanutti [a], Ali Abdollahzadeh [b], Fabio Mangini [a], Marta Moraschi [d], Inna Bukreeva [e,f], Lorenzo Massimi [e,1], Francesco Brun [e,g], Jussi Tohka [b], Olli Gröhn [b], Alberto Mittone [h], Alberto Bravin [i], Charles Nicaise [j], Federico Giove [d], Alessia Cedola [e], Michela Fratini [a,e,*]

[a] IRCCS Fondazione Santa Lucia, Roma, Italy
[b] A.I. Virtanen Institute for Molecular Sciences, University of Eastern Finland, Kuopio, Finland
[c] Institute of Nanotechnology, CNR, Rome Unit, Roma & Institute of Nanotechnology, CNR, Lecce Unit, Lecce, Italy
[d] MARBILab, CREF - Centro Ricerche Enrico Fermi, Roma, Italy
[e] Institute of Nanotechnology- CNR, Rome Unit, Piazzale Aldo Moro 5, Rome, Italy
[f] P.N. Lebedev Physical Institute, RAS, Leninskiy pr., 53 Moscow, Russian Federation
[g] Department of Engineering and Architecture, University of Trieste, Trieste, Italy
[h] CELLS- ALBA Synchrotron Light Source, Barcelona, Spain
[i] European Synchrotron Radiation Facility (ESRF), Grenoble, France
[j] URPhyM NARILIS, Université de Namur, Rue de Bruxelles, Namur, Belgium

ARTICLE INFO

Keywords:
X ray phase contrast tomography
Vascular network
3D steerable filter

ABSTRACT

Purpose
Image processing plays a fundamental role in the study of central nervous system, for example in the analysis of the vascular network in neurodegenerative diseases. Synchrotron X-ray Phase-contrast micro-Tomography (SXPCT) is a very attractive method to study weakly absorbing samples and features, such as the vascular network in the spinal cord (SC). However, the identification and segmentation of vascular structures in SXPCT images is seriously hampered by the presence of image noise and strong contrast inhomogeneities, due to the sensitivity of the technique to small electronic density variations. In order to help with these tasks, we implemented a user-friendly ImageJ plugin based on a 3D Gaussian steerable filter, tuned up for the enhancement of tubular structures in SXPCT images.
Methods
The developed 3D Gaussian steerable filter plugin for ImageJ is based on the steerability properties of Gaussian derivatives. We applied it to SXPCT images of ex-vivo mouse SCs acquired at different experimental conditions.
Results
The filter response shows a strong amplification of the source image contrast-to-background ratio (CBR), independently of structures orientation. We found that after the filter application, the CBR ratio increases by a factor ranging from ~6 to ~60. In addition, we also observed an increase of 35% of the contrast to noise ratio in the case of injured mouse SC.
Conclusion

* Corresponding author at: Institute of Nanotechnology- CNR, Rome Unit & IRCCS Fondazione Santa Lucia, Roma, Italy.
E-mail address: michela.fratini@gmail.com (M. Fratini).
[1] Present address: Department of Medical Physics and Biomedical Engineering, University College London, Gower St, London WC1E 6BT, UK.

https://doi.org/10.1016/j.ejmp.2020.12.010
Received 10 July 2019; Received in revised form 3 December 2020; Accepted 14 December 2020
Available online 17 January 2021

The developed tool can generally facilitate the detection/segmentation of capillaries, veins and arteries that were not clearly observable in non-filtered SXPCT images. Its systematic application could allow obtaining quantitative information from pre-clinical and clinical images.

1. Introduction

The segmentation of vascular networks (VNs) in the central nervous system (CNS) is of crucial importance for clinical and pre-clinical image processing applications (see, e.g., [1] for a review on this subject). In particular, the three-dimensional (3-D) analysis (determination of crucial parameters such as density, distribution and continuity of vessels) of the VN (including its smallest capillaries), is one of the key issues in neurodegenerative diseases, such as multiple sclerosis [2–4], where pathologic neurovascular alterations have been regarded as a key process [2,3]. In this framework, the knowledge of the relative spatial location of blood vessels with respect to neurons and axons is mandatory for improving our understanding of the effects of pathological processes.

To this aim, a 3-D high-resolution micro-imaging technique is required to define the complex structure of the VN in the central nervous system. Magnetic resonance angiography, volumetric computed tomography [5] and conventional X-ray angiography [6] have been used to image the neural vasculature, but their low resolution is inappropriate for imaging small vessels (<20 μm). High-resolution synchrotron tomography has been proposed for the complete 3D imaging of micro-VNs [6], yet a better contrast is achieved by imaging the phase modulation induced by an object in a coherent beam [7,8]. This latter feature makes Synchrotron X-ray Phase-contrast micro-Tomography (SXPCT) a very attractive method to study weakly absorbing samples and features (such as the spinal cord vascular and neuronal network) at the micron scale, without using contrast agent [7,9,10].

However, for phase-contrast tomography data the avoidance of contrast agents makes vessels difficult to segment using intensity-based image processing approaches, such as choosing an appropriate threshold within the distribution of intensity values in an image histogram, because the range of values characterizing the vessels strongly overlaps with those pertaining to other structures and to the background. In addition, the segmentation of VNs in SXPCT images is seriously hampered by the presence of image noise and of strong contrast inhomogeneities due to the sensitivity of the technique to small electronic density variations, as well as by the multi-scale nature of vessels and nerve fibres, which prevents from using size-based automated recognition algorithms. For all these reasons, a *tubular structures enhancer* is required in order to make an efficient 3D segmentation of the vascular network in SXPCT images.

Large varieties of methods have been set up, mostly of which relying on the morphological properties of "tubular structures". Very simple vessel detection techniques were developed many years ago (based on global or locally adaptive thresholds developed in a more general context [11,12]), and have been extensively used because of their conceptual simplicity and low computational cost. Their main drawback is the need of a careful fine-tuning in parameters selection to avoid inaccurate results. Recently, more sophisticated techniques have been introduced following an iterative approach in which, starting from a set of manually chosen "seed points", the segmentation proceeds propagating towards peripheral branches by means of active contours [13], region growing [14,15] and particle filtering or path tracing [16–19] thus exploiting the interconnected, "graph-like", topological structure of vessels.

However, a requisite building-block in such algorithms is the measure of tubular degree or "vesselness'', that is more commonly evaluated by means of Hessian-based methods. These rely on the eigenstate analysis of the Hessian, estimated from the second-order derivatives of local intensity levels, which can then be used to define a vesselness as a function of the eigenvalues [18,20–22]. Nonetheless, in order to deal with the multi-scale nature of vascular structures, Hessian-based filters usually include a preliminary Gaussian convolution that has to be re-applied each time at the different scales. This tends to blur vessel boundaries, which could make scale selection inaccurate, especially close to bifurcations. To overcome this issue various authors proposed more sophisticated versions of this approach, such as bi-Gaussian pre-filtering [23] and oriented flux calculations at the boundary of localized circles (2-D) or spheres (3-D) with different radii (i.e. scales) [24,25]. Unfortunately, these improvements imply a non-negligible computational extra-cost to pay for.

Alternative techniques to enhance tubular structures include optimal edge detection [11] and steerable filters [26,27]. Among these techniques, we chose to implement a Gaussian steerable filter [28] which, with respect to Standard 3D Gaussian filters, offers the possibility to enhance local features by using the steerability properties of Gaussian derivatives [28]. Conversely, standard 3D Gaussian filters are based on the convolution of a Gaussian distribution with the image, and are generally applied in a pre-processing step to blur images and to "average out" the noise. While this can make the edge detection easier, it also clearly results in a loss of image definition, which is absent in the images treated with our protocol.

In addition, the Steerable 3D filter allows to achieve a good compromise between computational cost [29] and features contrast enhancement. Indeed, this filter shows two important properties: i) it has an explicit scale parameter that allows us to optimize the filter response (FR) to take into account the multi-scale nature of vascular structures and ii) the filter convolution can be computed very efficiently for any arbitrary orientations thanks to the steerability property of Gaussian derivatives [18].

In this paper we describe the implementation of a 3D steerable Gaussian filter within the ImageJ integrated graphical platform (https://imagej.net) with the final aim to tune up a user friendly plugin that can be used to enhance tubular structures(i.e. vessels) in SXPCT images.

ImageJ is a public domain and open-source image processing software tool whose main strengths are modularity, portability and computational efficiency [28]. For these reasons, we decided to implement it as a (publicly available and open-source) plugin that can be integrated in the platform. To our knowledge no 3-D steerable filters are available as a plugin for ImageJ (see [27] for a 2D implementation). Finally, we report on various filter quality tests applied to SXPCT mouse spinal cord images and the application on spinal cord injured mouse model.

2. Materials and methods

2.1. Sample preparations

We studied 12 spinal cord samples from ex-vivo healthy adult male C57BL/6J mice (5–6 weeks old, weight 21–28 g, Charles River). The animals were housed in a room (22 ± 1 °C, 50%–60% humidity) with 12 h light/dark cycle and free access to food and water. The mice were anaesthetized intraperitoneally with a ketamine (80 mg/kg)/xylazine (10 mg/kg) mixture and perfused transcardially with 0.9% saline solution containing heparin (50 U/ml) for 3 min at 2 ml/min. After that, the mice were divided in 4 groups. The samples arising from one group were perfused with physiological solution; the ones from another were perfused with MICROFIL®, a low-viscosity radio-opaque polymer (Flowtech, Inc., Carver, Massachusetts) well suited for vascularization studies. In the case of the third group, the samples were perfused with

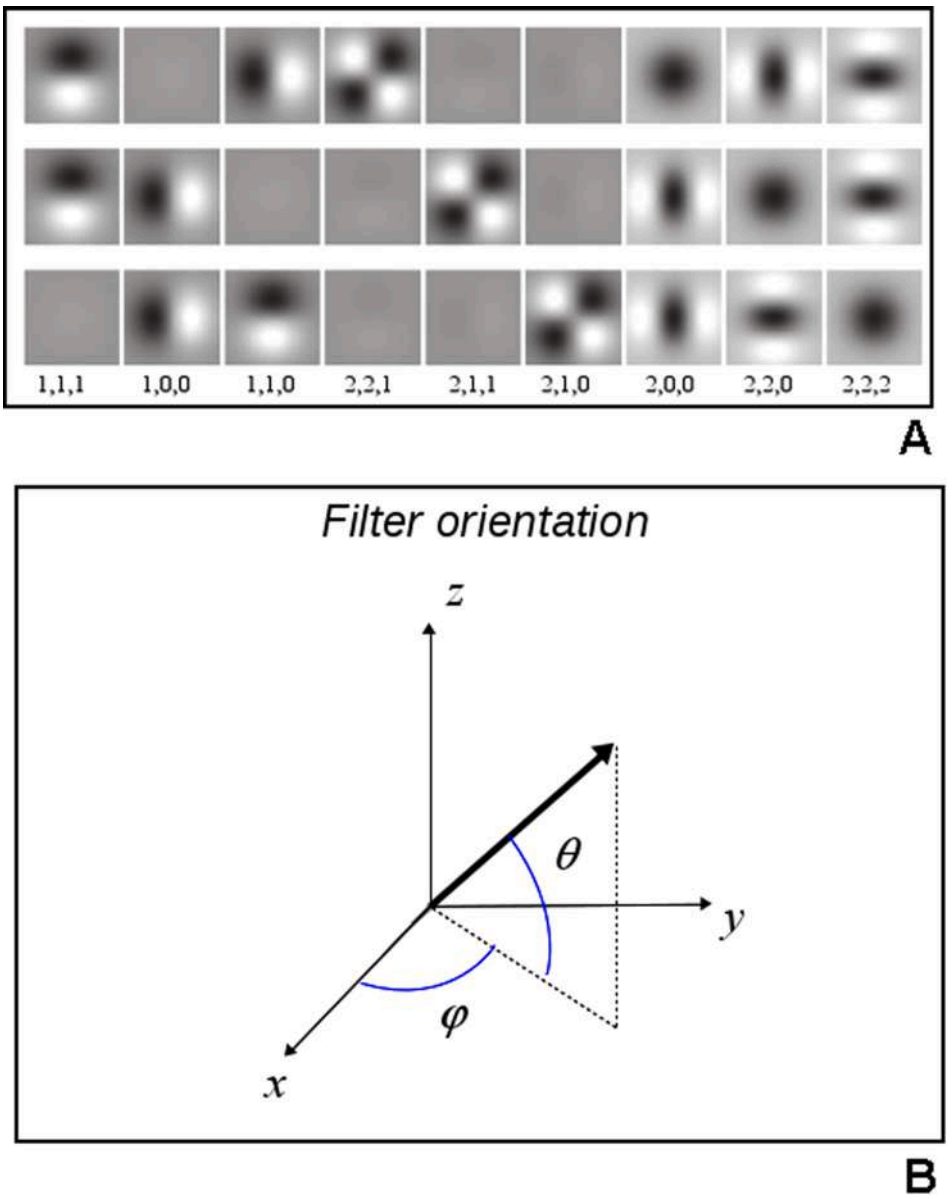

Fig. 1. A) Filter templates. From top to bottom: sagittal, coronal and axial central cross-sections of the filter templates for various orders of the normalized derivatives of Gaussians (as labelled at the bottom) and without rotation. The size of each cross-section is 6σ. The data are the results of computation done by following the eq. (1). **B) Filter 3D orientation**.: Elevation (θ) and azimuth (φ) determine the FT direction. The *xy* plane is parallel to each tomographic slice plane.

pure ethanol, while for the last group the samples were perfused with paraformaldehyde (PFA). The paraformaldehyde (PFA) solution was 4% in 0.1 M phosphate buffer saline (PBS). After the perfusion, the spinal cord of each mouse was extracted from the spine and placed in the incubation solution, i.e., PFA (4%) for the Microfil- and PFA-perfused mice and ethanol for the ethanol-perfused mice .The detailed sample preparation protocol is reported in [30]. These experimental animal procedures was be carried out at the A.I.Virtanen Institute for Molecular Sciences at the University of Eastern Finland (Kuopio, Finland) and approved by the Animal Care and Use Committee of the Provincial Government of Southern Finland and performed according to the guidelines set by the European Community Council Directive 86/609/EEC.

We also studied the spinal cord of a unilaterally contused mouse. The animal study protocol was conducted according to the European Guidelines for Animal Experiments (2010/63/EU, 86/609/EEC and 87–848/EEC) and was approved by the Animal Ethics Committee of University of Namur (UN 17–284). Spinal cord injury (i.e., ipsilateral hemicord) was induced in a mouse as already described [31]. A unilateral, right-sided, spinal contusion was applied, under anesthetized condition, at the C5 level using a computer-controlled spinal impactor with an impact force set at 50 kDyn (IH400, Infinite Horizon).

Thirty minutes after the injury, the mouse was anesthetized with ketamine (100 mg/kg) and xylazine (5 mg/kg) and euthanized by exsanguination and intracardiac perfusion with 0.9% NaCl followed by buffered 4% paraformaldehyde. The cervical spinal cord was harvested, post-fixed overnight in paraformaldehyde, and subsequently dehydrated in Sakura-Tissue Tek–VIP for paraffin-embedding.

SXPCT measurements

In-line SXPCT measurements were carried out at the I13-2 beamline of Diamond Light Source (Harwell Science and Innovation Campus, Oxfordshire, UK) and at the ID17 beamline of ESRF (Grenoble, France). At I13-2 tomographic images were collected using a pink beam, an intense filtered synchrotron radiation beams with a broad energy range [32,33] (which in our case was centered at 14.7 keV) and a system of magnification optics connected to a PCO.Edge 5.5 camera to get an

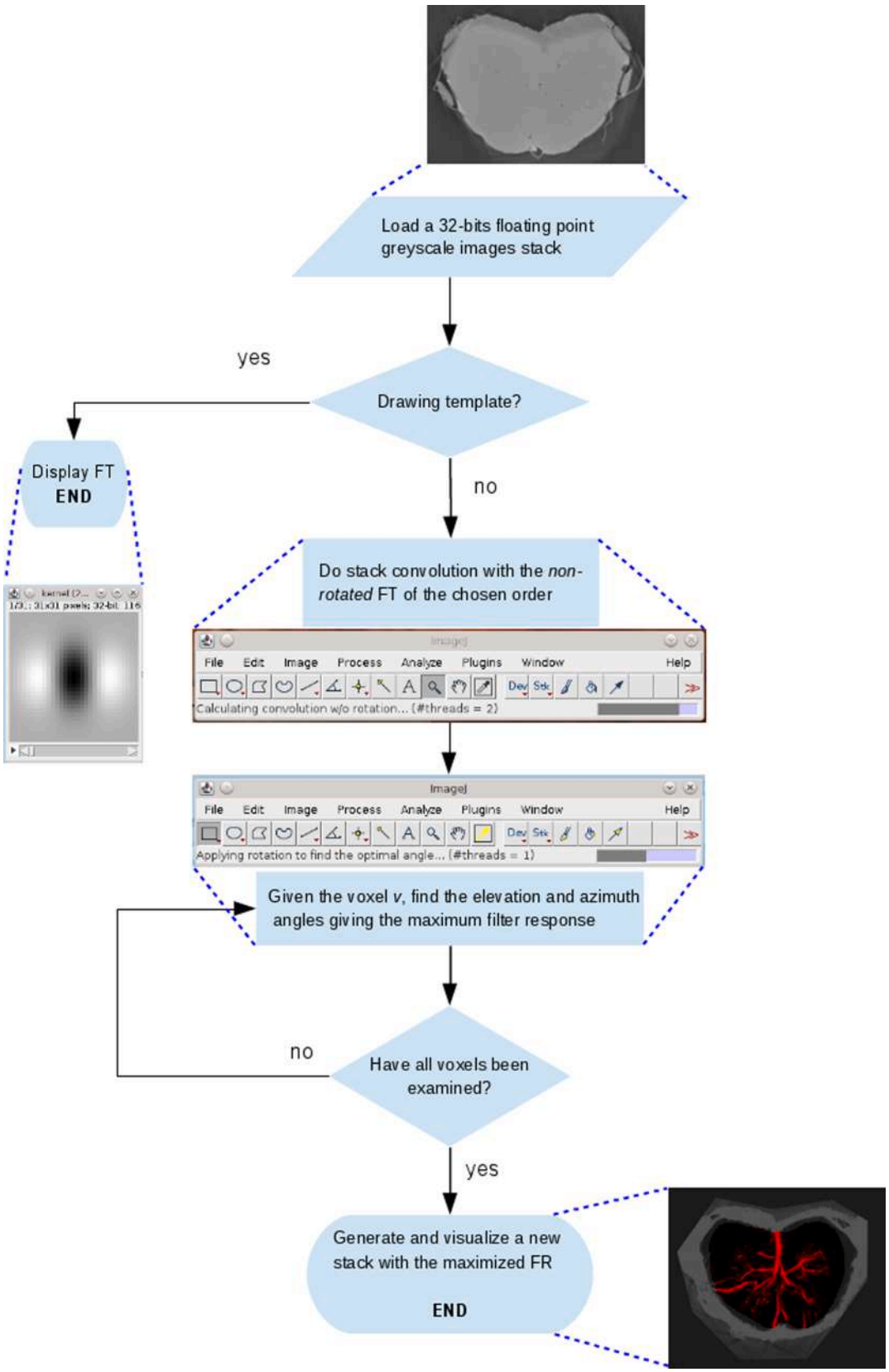

Fig. 2. Steerable3D workflow. Flowchart of the plugin working steps.

affective pixel size of 1.625 μm; the sample was located 70 cm far from the detector. At ID17 a monochromatic X-ray beam at the energy of 30 keV was used, in combination with a sample-detector distance of 2.0 m and a detection pixel size of 3.5 μm [34]. Energies and distances were chosen in order to enhance the intensity modulations induced by diffraction (rather than by attenuation) in a coherent or partially coherent beam [35] passed through- the object.

Phase retrieval was performed applying the single distance method proposed by Paganin [36] and all projections were processed and reconstructed using an open-source software tool SYRMEP Tomo Project [37]. We thus obtained a set of high-spatial resolution tomographic images, where the different grey levels are proportional to the electron density of the different tissues inside the sample [7,8].

The reconstructed volumetric images were analysed and filtered by means of ImageJ, using the home-developed plugin as described below.

2.2. The "Steerable3D" tool

The 3-D segmentation of the VN, up to the capillary network (on ~8 μm of length-scale), makes the adoption of a **computationally** efficient filter in 3-D of crucial importance for medical application. For this reason, we implemented a filter based on 3-D Gaussian derivatives which allows to filter along any arbitrary orientation with a small computational extra-cost. The result of the filtering procedure – the FR – is obtained by the convolution of the image with the filter template (FT, see Fig. 1 A). Specifically, the convolution consists in a weighted average of all the image pixels around a given one, with the weights given by the FT (see below). Moreover, the FT can be easily re-scaled so as to enhance vessels/fibres of different size (from ~1 to ~30 μm).

The filter implementation was done as a form of an ImageJ (open-source) plugin that we called "Steerable3D" (S3D). It is based on the theoretical approach described by Schneider and colleagues [27] in which the adopted FTs are written as normalized derivatives of Gaussians, that is:

$$G^{\sigma}_{M,a,b}(\vec{x}) = \sigma^{M}\frac{\partial^{M-a}\partial^{a-b}\partial^{b}}{\partial_x^{M-a}\partial_y^{a-b}\partial_z^{b}}G^{\sigma}(|\vec{x}|) \tag{1}$$

where the triplet (M, a, b), with $M > 0$, $0 \le a \le M$ and $0 \le b \le a$, identifies the template "order" and $G^{\sigma}(x)$ is the gaussian with variance σ^2 and zero mean. In Fig. 1 A, the form of the FT at various orders is illustrated.

In addition to having an explicit and easily adjustable scale parameter (σ), this filter is "steerable" also in 3-D (as was demonstrated in [28], see also [26,38]). Steerability is the property whereby the convolution of an image with a rotated version of the FT can be expressed as a linear combination of various orders of the same FT *without rotation*. In formal notation, given the FR, i.e. the convolution of the image I with the FT at the voxel $\vec{x}(x,y,z)$, as

$$f^{\sigma}_{M,a,b}(I,\vec{x}) = \left(I^{*}G^{\sigma}_{M,a,b}\right)(\vec{x}), \tag{2}$$

then the convolution with the FT rotated in 3D with a given elevation (θ) and azimuth (φ) angles (with respect to the axial, slice, xy plane, see Fig. 1 B) can be written as

$$f^{\sigma}_{M,a,b}(I,R\vec{x}) = \sum_{i=0}^{M}\sum_{j=0}^{i} w^{ij}_{M,a,b}(\theta,\varphi) f^{\sigma}_{M,i,j}(I,\vec{x}) \tag{3}$$

where $R = R(\theta, \varphi)$ is the corresponding rotation matrix and $w^{ij}{}_{,Ma,b}(\theta,\varphi)$ is a set of coefficients depending on the angles (Ref. [28], Sect. 2.1.2, for further details). As a consequence, for the sake of computational convenience and rapidity, the evaluation of the rotated FR can be done by using Eq. (3) instead of the direct and much more computational expensive convolution (2) re-evaluated at $R\vec{x}$. In the plugin, the optimal orientation is found for each voxel as that giving the maximum FR among the responses corresponding to the angles:

$$\begin{aligned}\theta &= \theta_1, \theta_1 + \Delta\theta, \theta_1 + 2\Delta\theta, \cdots, \theta_2\\ \varphi &= \varphi_1, \varphi_1 + \Delta\varphi, \varphi_1 + 2\Delta\varphi, \cdots, \varphi_2\end{aligned} \tag{4}$$

where the angular bounds $0 \le \theta_1 < \theta_2 \le 90°$, $0 \le \varphi_1 < \varphi_2 \le 360°$ and the steps $\Delta\theta$, $\Delta\varphi$ can be given by the user (see next Section). Notice that only one half-space (with $z \ge 0$) needs to be considered because all the FTs are invariant under the $\theta \to -\theta$ transformation.

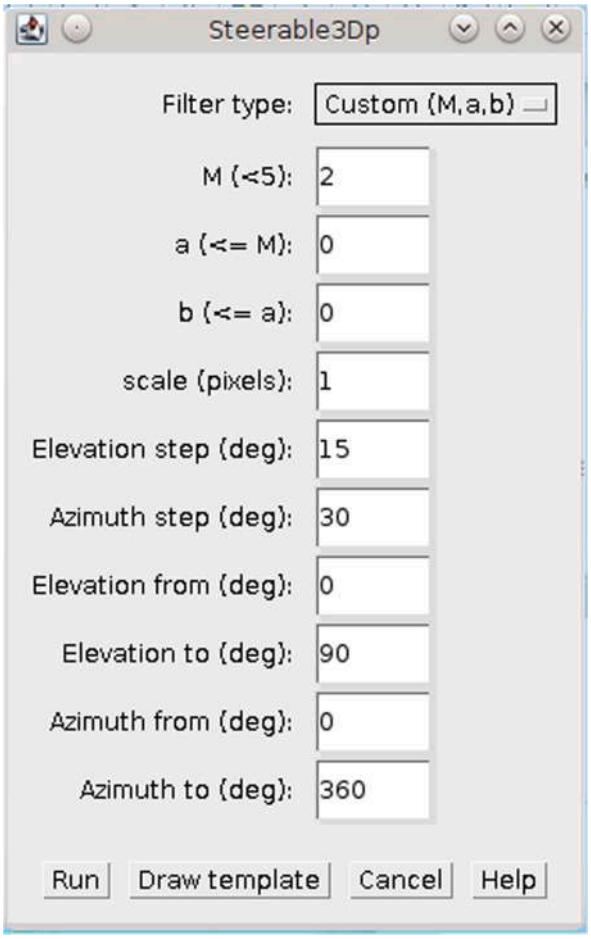

Fig. 3. Plugin GUI. 'Elevation step' refers to $\Delta\theta$; 'Azimuth step': $\Delta\varphi$; 'Elevation from': θ_1;'Elevation to': θ_1 'Azimuth from': $\varphi 2\square$ and 'Azimuth to': φ.

3. Results

3.1. The S3D workflow

The S3D plugin is written in Java and it is capable to run in parallel on multi-CPU computers thanks to the native multithreading mechanism of Java language. Since each thread can operate independently of each other on a subset of all the slices composing the 3-D stack, the computational parallelization can be done straightforwardly in both the calculation stages and the performance shows a good scalability (see Fig. 2 for a sketch of the tool workflow).

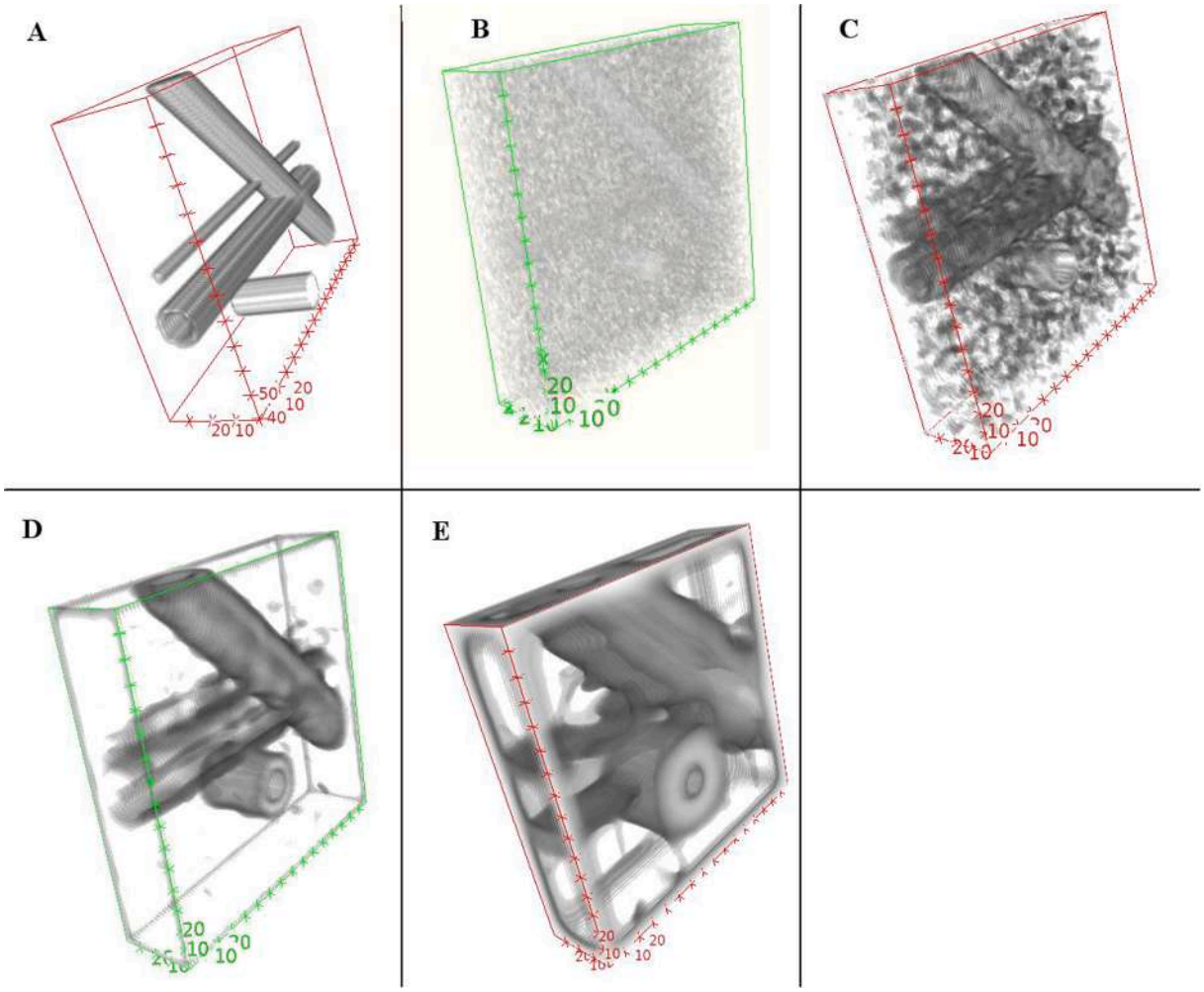

Fig. 4. Filtering a synthetic image. (A) Four synthetic "vessels" generated as cylinders of various size and orientation within a box of 140 × 140 × 60 pixels. They have either 8 or 2 voxels width. (**B**) The same as in (**A**) but with a white noise added with an average grey level equal to the grey level of the "vessels"; in this case a certain degree of transparency had to be set in the 3-D rendering to improve visibility. (**C, D, E**) FT (2,0,0) responses of the (**B**) volumetric image using a scale σ = 2, 4, 8, respectively.

S3D operates on 32-bit (single precision floating point) greyscale images, and therefore other types of images must be converted before being treated (ImageJ has an embedded conversion tool that is accessible through the Image -> Type menu path). Moreover, it needs 3D images, thus a stack of 2-D image slices must be loaded first. Then, the plugin can be launched and a GUI opens (Fig. 3). The user can first select whether to apply a "custom" FT order by giving the values for M, a and b, or to set a pre-defined FT. S3D provides three different pre-defined templates, namely: i) the "Edge" type that corresponds to (M, a, b) = (1,0,0) and yields an edge detector, ii) the "Ridge" type, with order (2,1,0), that gives a high response when a linear bright series of voxels is surrounded by darker voxels and iii) the order (2,0,0) that we name "Vessel" type because it yields a high response when a darker set of aligned voxels is confined within brighter "boundaries" (see Fig. 1 A). The user can then set the "scale" parameter (corresponding to σ in Eq. (1)), as a length-scale parameter for the FT, as well as the angular limits and the steps used in the search for the optimal filter orientation (Fig. 3).

When the "Run" button is pressed the plugin starts to calculate the filter convolution (without rotation, Eq. (2)) with the whole image. The progression of this stage is shown in the progress bar of the ImageJ main window (Fig. 2), along with the information on how many threads are being used in this calculation. After that, the searching for the optimal rotation angle is executed (applying Eq. (3)) while the progress bar and the number of threads are displayed also for this stage. At the end a new image stack is displayed containing the 3-D FR. Finally, notice that if the button "Draw template" is pressed, then the plugin will just display the chosen FT form; therefore only the filter order is taken into account in this case.

3.2. Steerable3D testing and application

For a proper comparison of the original volumetric images with the filtered ones we made a 2D projection of their voxels. Let x and y be the horizontal and vertical axes, respectively, on the spinal cord axial plane, so that the z-axis lies along the images stack axis (i.e. perpendicular to the axial plane). Each non-filtered volume of interest (VOI) was thus projected through the following steps:

1. taking the "projected minimum" of the VOI. This was done by creating a 2D image in which the grey level p of the generic pixel at (x, y) is given by

$$p(x,y) = \min_{0\le z\le Z}\{v(x,y,z)\} \tag{5}$$

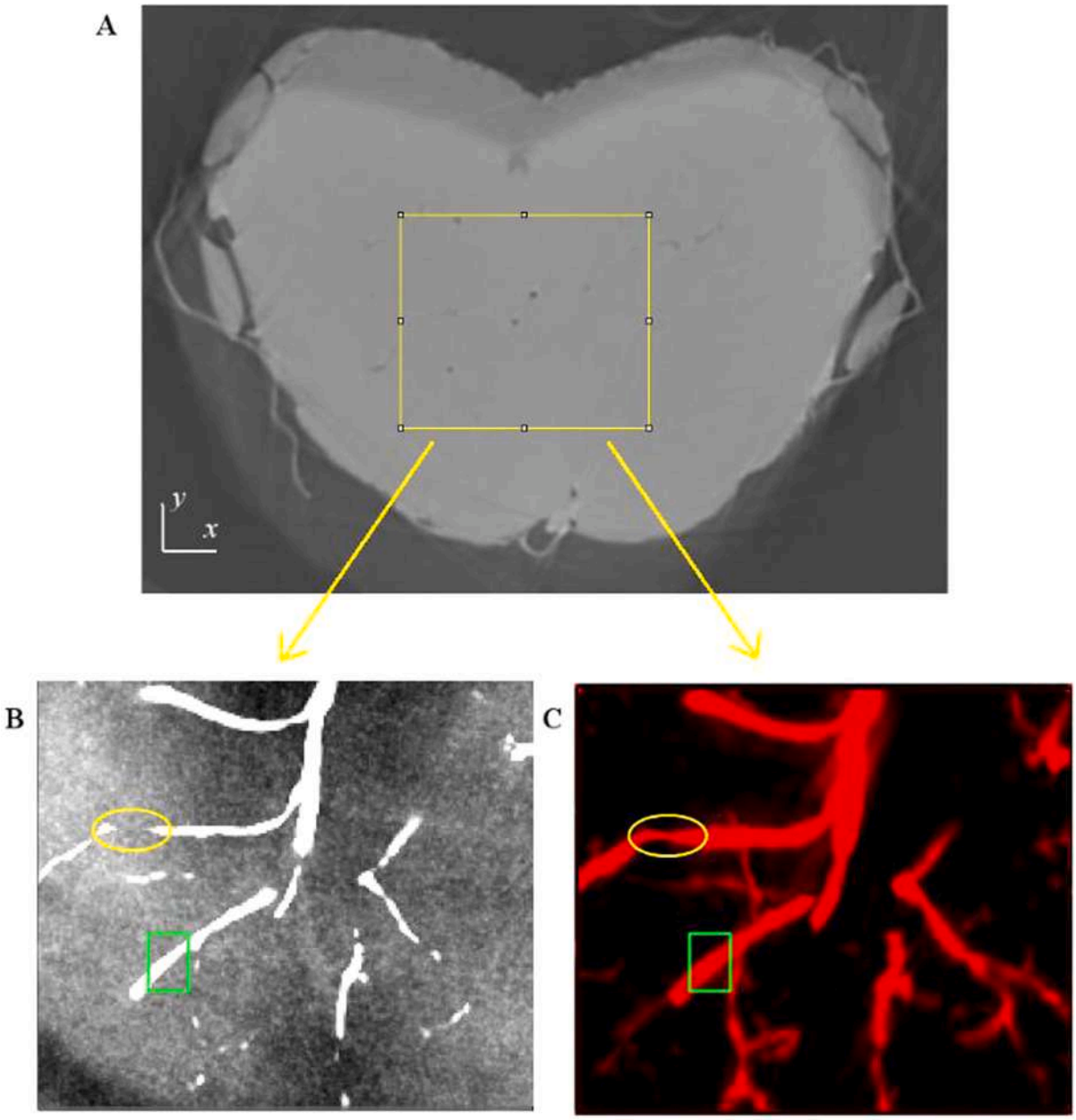

Fig. 5. Filter test on a SPCT image of a mouse spinal cord perfused with contrast agent (MICROFIL®**).** (**A**) Axial cross-section and a VOI with size 200 × 170 × 100 voxels (1 voxel size = 3.5 μm) enclosed in a yellow contour (the white scale bar is 150 μm). (**B**) Projection of the VOI of (**A**). (**C**) maximum projection of the S3D response stack (FT order 2,0,0 with σ = 2). The ramifications of the anterior (sulcal) artery are clearly visible. The green rectangles indicate the regions used to evaluate the CBR on a vessel (see text). Yellow ovals enclose a region in which a vessel discontinuity is revealed as only apparent by the FR contrast enhancement. (scale bar in **B** and **C** is 30 μm). (For interpretation of the references to colour in this figure legend, the reader is referred to the web version of this article.)

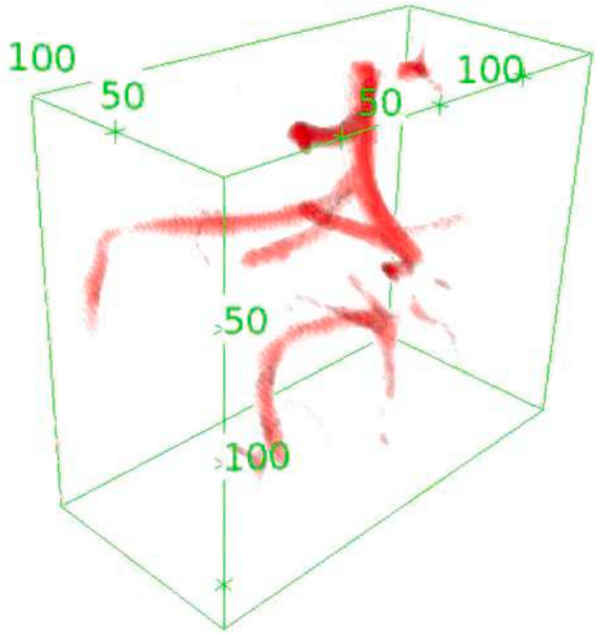

Fig. 6. Filter response 3-D rendering. Three-dimensional structure of the vascular network in the volumetric FR (projected in Fig. 5).

where $v(x, y, z)$ is the grey level of the VOI voxel at (x, y, z), with Z being the upper limit of the z coordinate (it coincides with the number of slices in the stack).

2. Taking the "projected maximum" of the VOI (i.e. applying Eq. (5), but with the "max" instead of the "min" operator).
3. Summing (pixel-by-pixel) the image of step (1) (after inverting their grey levels) with the projected maximum of step (2).

For grey scale "inversion" we mean the transformation of the grey level p of a pixel to $M - p + m$, with m and M being, respectively, the minimum and maximum grey level of the image (notice that the absolute value of the difference between the grey levels of any pixels pair is invariant under this transformation).

Indeed, the projected minimum and maximum are commonly used to segment projected neurovascular network in images stack (see, e.g. ref. [2,9]) because, on the one hand, the resulting dark pixels very likely come from vessels lumen and, on the other hand, cell bodies tend to give rise to bright pixels. Moreover, as we will see below, since in the filtered image the vessels' pixels are *brighter* than the background, we transformed the dark vessels of the non-filtered image into bright objects by inverting the projected minimum, so to make the image more easily and visually comparable with the projected FR. The latter was obtained by doing only the "projected maximum" on the 3-D FR voxels. Indeed, the grey level in the FR can be regarded as a "vesselness" measure.

As a first step, we applied S3D to simple synthetic images (Fig. 4 A). In Fig. 4 B we can see a 3-D view of synthetic "vessels" represented by cylinders immersed in additive white noise (in Fig. 4 A the "vascular network" is reported without noise for illustrative purposes). The size of vessels was either 2 or 8 voxels. In Fig. 4 C, D, E the FRs are reported for the "Vessel" FT (order 2,0,0) with scale parameter $\sigma = 2$, 4 and 8, respectively. We can see that the filter behaves as expected, as it enhances the contrast between vessels walls and the (noisy) background. It is also apparent that the scale parameter must be chosen wisely, depending on the noise level and on the size of the features we wish to enhance/discriminate. In this respect, it is worth noting that in Panel E the internal calibre of the cylinders image appears reduced (and the thickness of the cylinders' walls seems increased) because the threshold for vessel edge detection is rather low, and due to the blurring of the original image the edge detection algorithm wrongly sets the positions of the external and internal surfaces of the vessels' walls.

As a realistic test of S3D, we examined SXPCT images. For the easiest comparison of the original volumetric images with the filtered ones, we made a 2D projection of their voxels. Specifically, we took the "projected minimum" and the "projected maximum" of the VOI from the non-filtered image stack (as commonly done to segment projected VN [2,9]). Then, we summed, pixel-by-pixel, the *inverted* grey levels of the former with those of the latter, where the inverted grey levels were calculated as previously described (ref. to sec. "SXPCT measurements) in order to turn dark pixels (which mainly correspond to vessel lumens) into bright ones. Finally, only the projected maximum was applied to the filtered VOI.

In Fig. 5 A, we selected a small VOI in the central part of a stack of 100 greyscale slices of a mouse spinal cord injected with MICROFIL® (this sample was measured at ID17 with a pixel size of about 3.5 μm)

In Fig. 5 B,C we can see how in the S3D response of the VOI the blood vessels contrast is clearly enhanced against the background pixels, revealing more details and vascular network connections. The non-filtered projected image was obtained through the above-described procedures, while the FR projected in Fig. 5 C was obtained by doing only the "projected maximum" on the 3-D FR voxels. The image in Fig. 5 C was rendered in red and, finally, in Fig. 6 the FR is rendered in 3-D to appreciate the filtered vessels global structure (using ImageJ and Amira_FEI 6.4 software).

In Fig. 7 the same comparison between non-filtered and filtered images was done in the same spinal cord region, on samples without contrast agent but only perfused with PFA or ethanol (these samples were measured at I13 with a pixel size of 1.6 μm) used as fixative agents [30]. Also in this case the filter greatly improves the general visibility of both blood vessels and neural fibres in the white matter region (we notice how the nerve fibres visibility is especially enhanced in the ethanol perfused specimen, Fig. 7 C,D).

The enhancement of the neurovascular system components that is apparent in the above-reported SXPCT images, can be rigorously quantified by measuring the contrast-to-background ratio (CBR, see. e. g., Ref. [39]). This can be defined as

$$c_X = \frac{S_X - B_X}{|B_X|} \tag{6}$$

where the 'X' index represents the component – or detail – we are interested in, S_X is the *maximum* grey level in the set of pixels within a region enclosing a significant part of that component and of the adjacent area (see, e.g., Fig. 7), and B_X is the background level, determined by taking the *minimum* grey level within the same region in which S_X was taken (of course $S_X \geq B_X$ by definition). In the following Table 1, X = 'V' stands for blood vessels and 'I' for the whole image.

We evaluated c_X both in the non-filtered image and in the filter response ($c_{X,FR}$), thus obtaining a sort of 'filter gain' defined as the ratio $c_{X,FR}/c_X$. This gain measures the "efficiency" of the filter application, i.e. how many times it increases the CBR of the relevant details with respect to their surroundings. Of course, care was taken to ensure that the same component and the same region were considered in both the filtered and non-filtered image to evaluate S_X and B_X. Resulting values are reported in Table 1.

In order to show its potential for pre-clinical applications, the S3D filter has also been also applied to tomographic images of an injured mouse spinal cord prepared without any contrast agent. Also in this case, we report non-filtered (Fig. 8 A) and filtered (Fig. 8 B) images. In order to help the comparison with healthy samples (see above), a slab of 320 μm was selected for filtering in all images. In this case, we also evaluated the CBR inside the small areas highlighted in green, for both not filtered and filtered images (C, D). In addition, we observe a 35% of contrast- to-

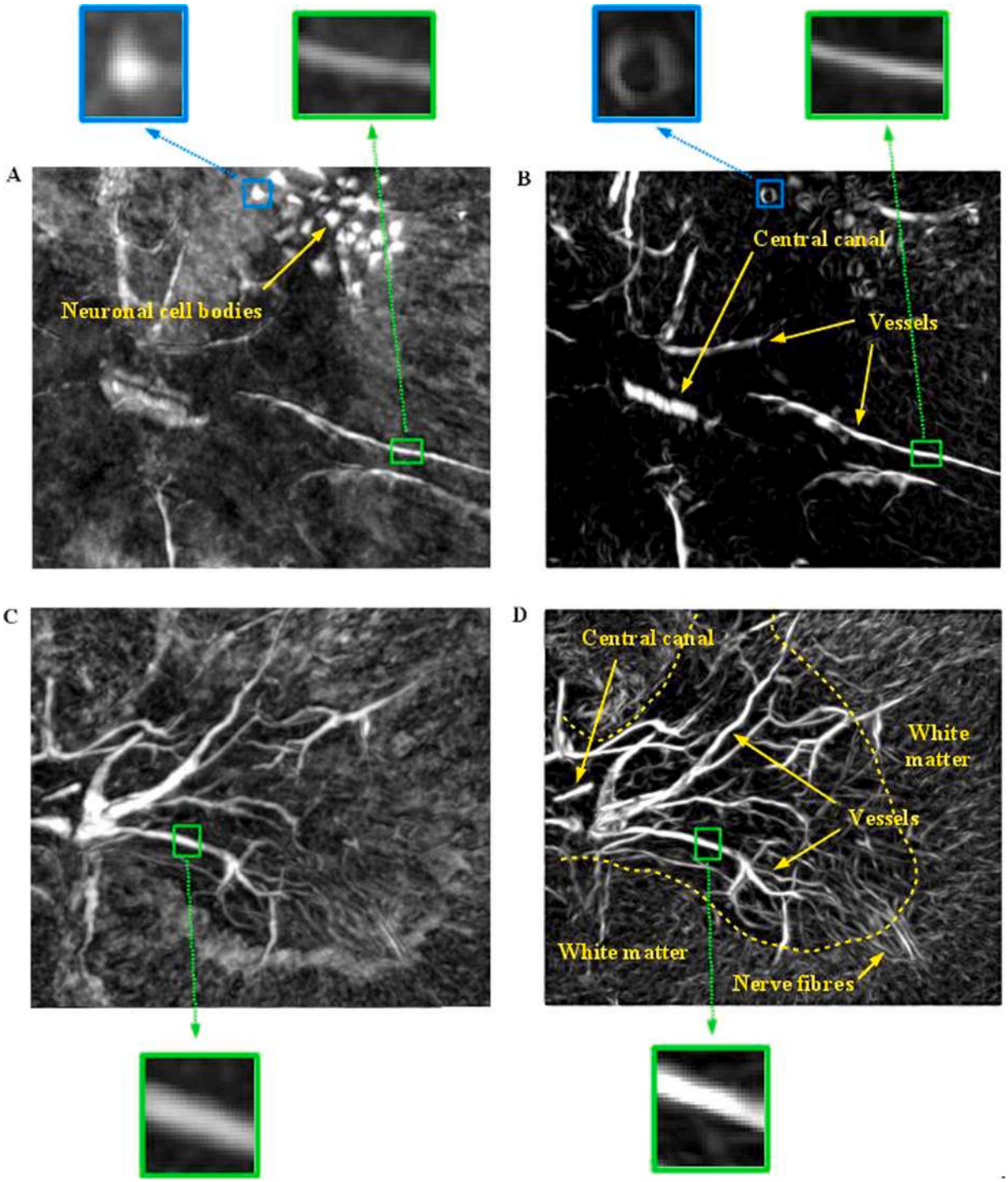

Fig. 7. Filter test on SPCT images of a mouse spinal cord without contrast agent. (A) Projected VOI (see text) with size 500 × 440 × 200 pixels (pixel size = 1.6 μm) in the same region as in Fig. 5 of a PFA perfused spinal cord. (B) Projected maximum of the FR stack of the VOI (FT order 2,0,0 with σ = 2). (C), (D) The same as (A) and (B), respectively, but with ethanol perfusion. The yellow dashed curve roughly delimits white and grey matters. The small rectangular regions used for the CBR calculation on a vessel (green) and a neuron (blue) are also enlarged and reported. In (D) the dense neural fibres network appears to be resolved in the white matter region. (white scale bar 20 μm). (For interpretation of the references to colour in this figure legend, the reader is referred to the web version of this article.)

Table 1
Contrast-to-background ratios and filter gain. List of measured contrast-to-background ratios, and corresponding filter gain, for the images presented in this work (as labelled in the first column). The subscript 'FR' denotes the CBRs as determined on the FR maximum projected image.

Figures	$c_{V,FR}$ /c_V	$c_{I,FR}$ /c_I	Note
5B,C	56.1/3.35 = 17	40.9/5.99 = 6.8	Microfil®
7A,B	3.35/0.0572 = 57	3.08/0.110 = 28	PFA perf.
7C,D	6.28/0.125 = 50	5.81/0.174 = 33	Ethanol perf.
8C,D	0.58/0.034 = 17		Fixed in paraformadehyde

noise ratio (CNR) increase as a consequence of the filter application.

Another possible application of this filter is to provide support for grey matter (GM) segmentation in spinal cords. Indeed, the differences in the vascular network structure between GM and white matter, yields a substantially different response, as we can see in Fig. 9. It is evident that the GM is globally more clearly distinguishable in the projected maximum of the FR (Fig. 9 B) than in the projected maximum (Fig. 9 A) of the original non-filtered stack. In particular, the FR gives rise to a rather sharp region with a peculiar pixels "texture" corresponding to the GM region, which can thus be more easily segmented.

4. Discussion

One of the challenges in VN segmentation is to underline variations in the vascular network morphology occurring in pathological states. In this sense, we need a high-resolution technique such as SXPCT -allowing to map the 3D arrangement of vascular details- together with an "optimal" segmentation algorithm, able to separate and recover information from a noisy image.

In this work the implementation of "Steerable3D", a 3-D steerable Gaussian filter for the visual enhancement of multi-scale neurovascular networks in 3D, is described and tested. The implementation is done in form of a publicly available, open-source and user-friendly plugin for the ImageJ modular software platform [40]. We preliminarily checked the filter response on a synthetic "vascular" image (represented by tubular structures) and we verified that S3D is able to extract and enhance the tubular features from the background. Moreover, we tuned up for the first time the Steerable Filter for high-resolution SXPCT images and we tested it on ex-vivo mouse spinal cord to show the performances of the filter under realistic conditions (differing in sample preparation and

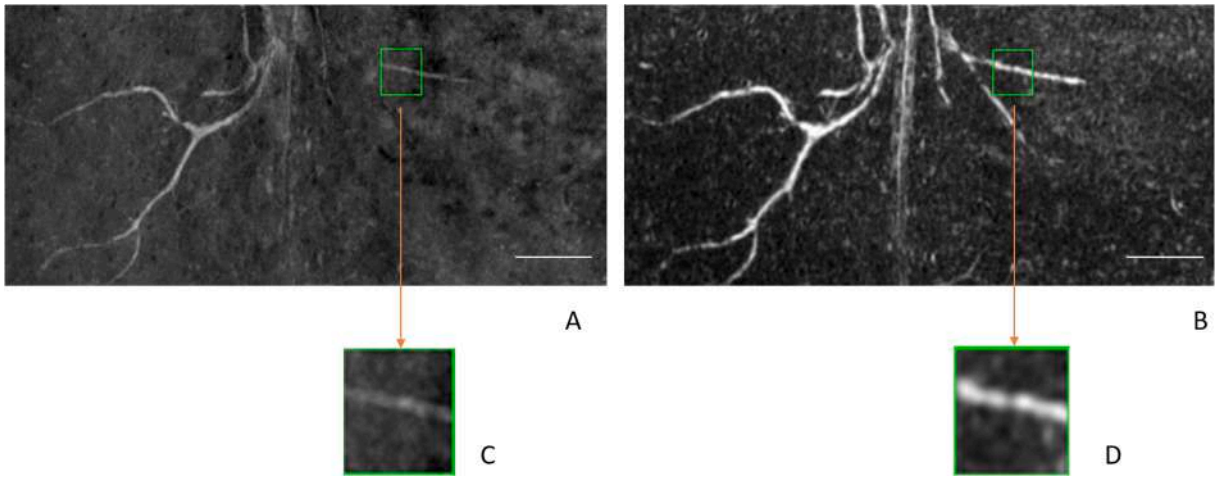

Fig. 8. Filter test on SXPCT images of a contralateral injured mouse spinal cord without contrast agent. (A) Projected VOI (see text) with size 540 × 241 × 100 pixels (pixel size = 3.09 μm) of a 30 min injured mouse spinal cord. (B) Projected maximum of the FR stack of the VOI (FT order 2,0,0 with σ = 2). The scale bar in white is of 200 um. The small rectangular green boxes represents the regions in which CBR and CNR computations have been performed. (For interpretation of the references to colour in this figure legend, the reader is referred to the web version of this article.)

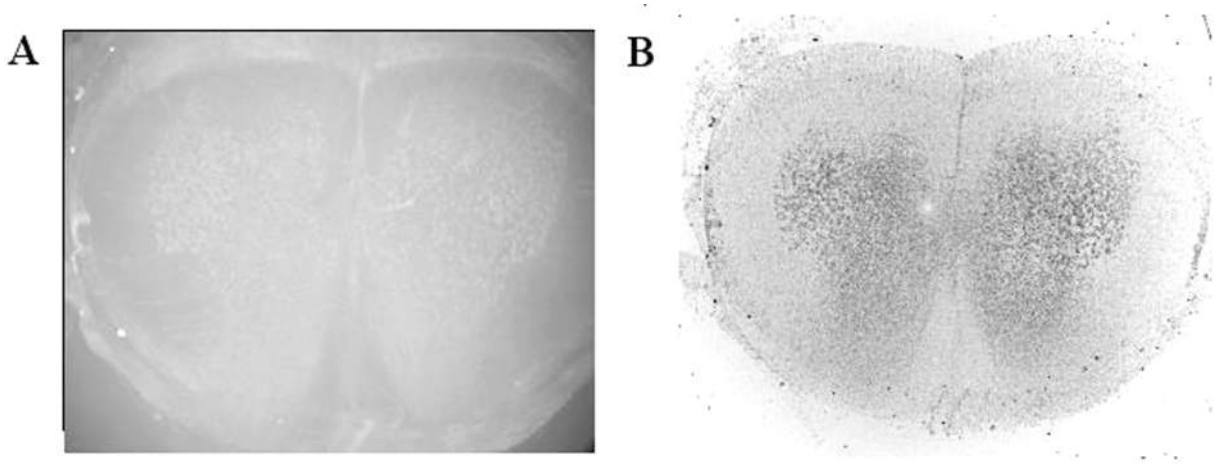

Fig. 9. Filter response on grey/white matter. (A) Projected maximum of a 200 SXPCT slices stack of a mouse spinal cord. (B) Projected maximum of the S3D volumetric response of (A).

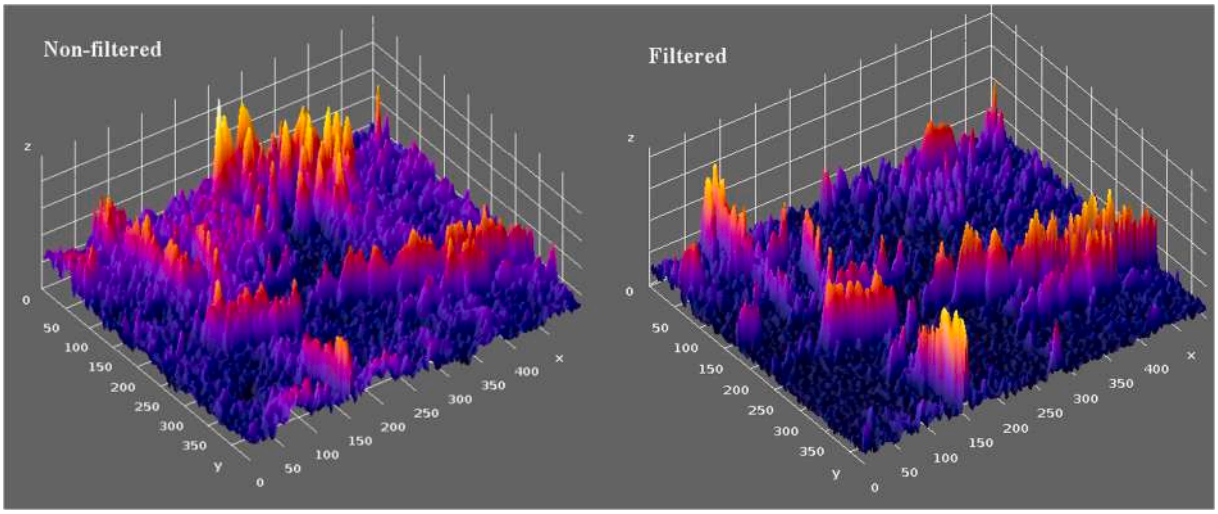

Fig. 10. Grey levels surface plot of the PFA perfused case. For each pixel at (x,y) in Fig. 9A and 9B, the grey level is reported on the z-axis in the non-filtered and filtered plot, respectively.

sample conditions, X-ray source and resolution). The tests confirm that S3D is able to enhance the visibility of blood vessels nerve fibres against the background voxels. This enhancement is confirmed by the comparison of the CBR measured before and after the filter application.

Values found for this ratio are listed in Table 1, where we can see that for blood vessels S3D can amplify the CBR ratio by a factor that ranges from ~6 to ~60, depending on the sample preparation/condition. Besides this, we tested the statistical significance of the visibility enhancement by means of a paired *t*-test on the $c_{x,FR}$ and c_x values from Table 1. In this case we found a p value = 0.1 for 8 degrees of freedom.

The above mentioned CBR can be visually and qualitatively understood also by observing the distribution of grey levels in the image pixels, reported in Fig. 10. The surface plot depicted in the figure refers to PFA-perfused case images. On the *z*-axis the grey level of every pixel in (x, y) of the images in Fig. 7 A,B is reported. We can immediately see that the "ranges of peaks" are higher and sharper in the filtered image than in the non-filtered one, with respect to the surrounding "valleys" of the surface plot. The lower grey levels associated to neurons in the FR in this case can be explained by the relatively high resolution of the image that allows to better reproduce the "irregular" ("starred") form of their soma, thus generating lower vesselness values in the FR.

In addition, the S3D tool provides an increase of the contrast to background ratio when applied to tomographic images of injured mouse spinal cord as suggested by the visible recover of vessel details (Fig. 8 C, D).

Recently, other methods have been used to enhance and recover information on tubular structures in SXPCT images. Among these, Tendero and colleagues used a seeded segmentation module available on the ilastic software in order to perform coronary segmentation in the heart tissue of a rabbit. Even if the method offers good results, it is limited by the fact that the user needs to define inside and outside "seeds" as an input to propagate inside the volume, making the procedure quite long and not really automated [41]. In addition, the method has only been applied to rabbit heart tomography, where the the structures are more visible because of their size and of a better contrast due to the biological composition of the tissue.

However, even if other algorithms have been already tuned up for segmenting conventional tomographic images, none of these had been successfully applied to SXPCT. In Fig. 11, for instance, we show a comparison between different vessel segmentations, resulting from the application of Steerable 3D, 3D Gaussian blurring and Frangi Filter 3D. In this case, we demonstrated a higher specificity of S3D in enhancing tubular structures with respect to the background when compared to the Frangi Filter 3D or to standard 3D Gaussian blurring.

In this paper, we have demonstrated for the first time that the S3D algorithm provides good results when applied to SXPCT in both normal and injured tissue. The obtained results could be useful in preclinical applications aimed at identifying damages occurring at the vascular level in the case of neurodegenerative diseases.

5. Conclusion

In summary and conclusion, the "Steerable3D" (S3D) filter, was developed to enhance the visibility of multi-scale vascular network in three-dimensional SXPCT images. The tests, carried out on high-resolution SXPCT images of ex-vivo healthy and injured mouse spinal cord, demonstrated that S3D can generally facilitate the detection/segmentation of smallest blood vessels, connections and axonal bundles that were not clearly observable in the non-filtered images.

It is worth mentioning that in its present version, S3D does not exploit the information about the template orientation that the employed algorithm uses internally to search for the best local response. In a forthcoming version of the tool, we plan to use this information with a twofold aim: i) as a guide for a skeletonization procedure (the optimal angles naturally indicate the main vessel/fibre local orientation), ii) to help discriminating vessels and nerve fibres as illustrated in Fig. 7.

Another possible application of S3D is to use it as a 'global' segmentation tool for white/grey matter in SC. Indeed, the very different nerve fibres and blood vessels density in the two regions lead to a rather different filter global response, which appear as regions with a very different graphical "texture" (see Fig. 9), thus allowing to distinguish between each other much more easily than in the original non-filtered image.

Finally, we remark the importance of having developed an *open-source* tool that can be easily extended/updated – also by contributors coming from the scientific community – in order to improve selectivity for the segmentation of the relevant features and to increase computational efficiency.

Declaration of Competing Interest

The authors declare that they have no known competing financial interests or personal relationships that could have appeared to influence the work reported in this paper.

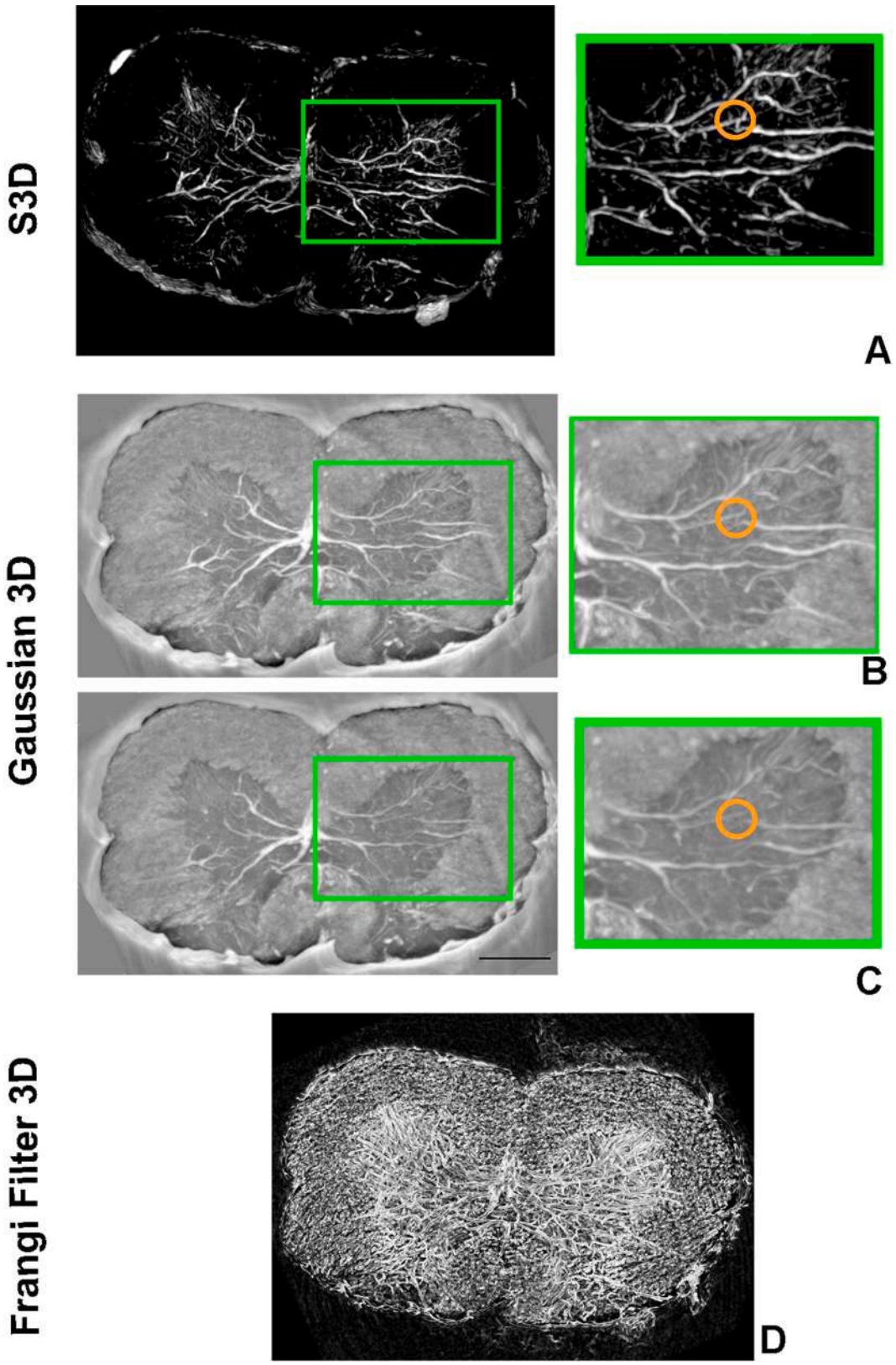

Fig. 11. Filter test on SXPCT images of a mouse spinal cord without contrast agent by using S3D (A), 3D isotropic Gaussian blurring (B, sigma = 2 along the three dimensions) and 3D anisotropic Gaussian blurring (C,$sigma_{x,y} = 2$, $sigma_z = 7$) and 3DFrangi Filter (D) Images represents the maximum intensity projection resulting from filtered images (slab thick 300 μm, scale bar 300 μm). In the right side of panels A,B,C an enlargement of the green selected area is shown in order to visualize differences in the application of the filters. In addition, some visible differences have been highlighted in orange circles. (For interpretation of the references to colour in this figure legend, the reader is referred to the web version of this article.)

Acknowledgements

Authors wish to thank the I13-2 and ID17 beamlines staff, at the Diamond Light Source and ESRF, respectively, for their helpful scientific and technical support. In addition, they would like to thank Maarit Pulkkinen for her help with the animal handling. Finally, the authors warmly thank Simone Melchionna, Marco Montuori for the helpful discussions on image processing algorithms and M. Felici for his critical reading of the manuscript.

Funding: This work was funded by the Italian Ministry of Health [Young Researcher Grant 2013, GR-2013-02358177] and by the European Union's Horizon 2020 research and innovation programme under the Marie Skłodowska-Curie grant agreement No 691110 (MICROBRADAM). In addition part of the project was financially supported by The FISR Project "Tecnopolo di nanotecnologia e fotonica per la medicina di precisione" (funded by MIUR/CNR, CUP B83B17000010001) and the TECNOMED project (funded by Regione Puglia, CUP B84I18000540002).

A. Sierra also acknowledges the Academy of Finland (#275453) for financial support. A. Bravin acknowledges COST Action CA16122 (BIONECA) and CNR Italy for financial support. Finally M. Fratini , t t the COST Action CA16122 "Biomaterials and advanced physical techniques for regenerative cardiology and neurology is acknowledged for networking support.

References

[1] Lesage D, Angelini ED, Bloch I, Funka-Lea G. A review of 3D vessel lumen segmentation techniques: Models, features and extraction schemes. Med Image Anal 2009;13:819–45.
[2] Cedola A, Bravin A, Bukreeva I, Fratini M, Pacureanu A, Mittone A, et al. X-ray phase contrast tomography reveals early vascular alterations and neuronal loss in a multiple sclerosis model. Sci Rep 2017;7:5890.
[3] MacMillan CJ, Starkey RJ, Easton AS. Angiogenesis is regulated by angiopoietins during experimental autoimmune encephalomyelitis and is indirectly related to vascular permeability. J Neuropathol Exp Neurol 2011;70:1107–23.
[4] Massimi L, Fratini M, Bukreeva I, Brun F, Mittone A, Campi G, et al. Characterization of mouse spinal cord vascular network by means of synchrotron radiation X-ray phase contrast tomography. Physica Med 2016;32:1779–84.
[5] Siegel A, Sapru H. Essential neuroscience. 2nd revised ed. Philadelphia: Lippincott Williams and Wilkins; 2011.
[6] Risser L, Plouraboué F, Steyer A, Cloetens P, Le Duc G, Fonta C. From homogeneous to fractal normal and tumorous microvascular networks in the brain. J Cereb Blood Flow Metab 2007;27:293–303.
[7] Bravin A, Coan P, Suortti P. X-ray phase-contrast imaging: from pre-clinical applications towards clinics. Phys Med Biol 2012;58:R1.
[8] Momose A, Takeda T, Itai Y, Hirano K. Phase–contrast X–ray computed tomography for observing biological soft tissues. Nat Med 1996;2:473.
[9] Fratini M, Bukreeva I, Campi G, Brun F, Tromba G, Modregger P, et al. Simultaneous submicrometric 3D imaging of the micro-vascular network and the neuronal system in a mouse spinal cord. Sci Rep 2015;5:8514.
[10] Maugeri L, DiNuzzo M, Moraschi M, Nicaise C, Bukreeva I, Mangini F, et al. Fractal dimension analysis of high-resolution X-ray phase contrast micro-tomography images at different threshold levels in a mouse spinal cord. Condensed Matter. 2018;3:48.
[11] Canny JF. Finding edges and lines in images. Massachusetts Inst of Tech Cambridge Artificial Intelligence Lab; 1983.
[12] Otsu N. A threshold selection method from gray-level histograms. IEEE Transactions on Systems, Man, and Cybernetics. 1979;9:62–6.
[13] Lorigo LM, Faugeras OD, Grimson WEL, Keriven R, Kikinis R, Nabavi A, et al. Curves: Curve evolution for vessel segmentation. Med Image Anal 2001;5:195–206.
[14] Lo P, Sporring J, Ashraf H, Pedersen JJ, de Bruijne M. Vessel-guided airway tree segmentation: A voxel classification approach. Med Image Anal 2010;14:527–38.
[15] Martínez-Pérez ME, Hughes AD, Stanton AV, Thom SA, Bharath AA, Parker KH. Retinal blood vessel segmentation by means of scale-space analysis and region growing. International Conference on Medical Image Computing and Computer-Assisted Intervention: Springer 1999:90–7.
[16] Florin C, Paragios N, Williams J. Globally optimal active contours, sequential Monte Carlo and on-line learning for vessel segmentation. European Conference on Computer Vision: Springer 2006:476–89.
[17] Lesage D, Angelini ED, Bloch I, Funka-Lea G. Medial-based Bayesian tracking for vascular segmentation: Application to coronary arteries in 3D CT angiography. In: 2008 5th IEEE International Symposium on Biomedical Imaging: From Nano to Macro: IEEE; 2008. p. 268–71.
[18] Schneider M, Sundar H. Automatic global vessel segmentation and catheter removal using local geometry information and vector field integration. In: 2010 IEEE International Symposium on Biomedical Imaging: From Nano to Macro: IEEE; 2010. p. 45–8.
[19] Zhou J, Chang S, Metaxas D, Axel L. Vascular structure segmentation and bifurcation detection. In: 2007 4th IEEE International Symposium on Biomedical Imaging: From Nano to Macro: IEEE; 2007. p. 872–5.
[20] Frangi AF, Niessen WJ, Vincken KL, Viergever MA. Multiscale vessel enhancement filtering. International conference on medical image computing and computer-assisted intervention: Springer; 1998. p. 130-7.
[21] Hernández-Vela A, Gatta C, Escalera S, Igual L, Martin-Yuste V, Radeva P. Accurate and robust fully-automatic QCA: method and numerical validation. International Conference on Medical Image Computing and Computer-Assisted Intervention: Springer; 2011. p. 496-503.
[22] Sato Y, Nakajima S, Shiraga N, Atsumi H, Yoshida S, Koller T, et al. Three-dimensional multi-scale line filter for segmentation and visualization of curvilinear structures in medical images. Med Image Anal 1998;2:143–68.
[23] Xiao C, Staring M, Wang Y, Shamonin DP, Stoel BC. Multiscale bi-Gaussian filter for adjacent curvilinear structures detection with application to vasculature images. IEEE Trans Image Process 2012;22:174–88.
[24] Benmansour F, Cohen LD. Tubular structure segmentation based on minimal path method and anisotropic enhancement. Int J Comput Vision 2011;92:192–210.
[25] Law MW, Chung AC. An oriented flux symmetry based active contour model for three dimensional vessel segmentation. European conference on computer vision: Springer; 2010. p. 720-34.
[26] González G, Aguet F, Fleuret F, Unser M, Fua P. Steerable features for statistical 3D dendrite detection. International Conference on Medical Image Computing and Computer-Assisted Intervention: Springer; 2009. p. 625-32.
[27] Jacob M, Unser M. Design of steerable filters for feature detection using canny-like criteria. IEEE Trans Pattern Anal Mach Intell 2004;26:1007–19.
[28] Schneider M, Hirsch S, Weber B, Székely G, Menze BH. Joint 3-D vessel segmentation and centerline extraction using oblique Hough forests with steerable filters. Med Image Anal 2015;19:220–49.
[29] Shrivakshan G, Chandrasekar C. A comparison of various edge detection techniques used in image processing. Int J Comput Sci Issues (IJCSI). 2012;9:269.
[30] Stefanutti E, Sierra A, Miocchi P, Massimi L, Brun F, Maugeri L, et al. Assessment of the effects of different sample perfusion procedures on phase-contrast tomographic images of mouse spinal cord. J Instrum 2018;13:C03027.
[31] Nicaise C, Putatunda R, Hala TJ, Regan KA, Frank DM, Brion J-P, et al. Degeneration of phrenic motor neurons induces long-term diaphragm deficits following mid-cervical spinal contusion in mice. J Neurotrauma 2012;29:2748–60.
[32] Mittone A, Fardin L, Di Lillo F, Fratini M, Requardt H, Mauro A, et al. Multiscale pink-beam microCT imaging at the ESRF-ID17 biomedical beamline. J Synchrotron Radiat 2020;27.
[33] Mark R. 2016;https://spie.org/news/6674-synchrotron-pink-beam-tomography-for-the-study-of-dynamic-processes?SSO=1.
[34] Mittone A, Manakov I, Broche L, Jarnias C, Coan P, Bravin A. Characterization of a sCMOS-based high-resolution imaging system. J Synchrotron Radiat 2017;24:1226–36.
[35] Cloetens P, Barrett R, Baruchel J, Guigay J-P, Schlenker M. Phase objects in synchrotron radiation hard x-ray imaging. J Phys D Appl Phys 1996;29:133.
[36] Paganin D, Mayo S, Gureyev TE, Miller PR, Wilkins SW. Simultaneous phase and amplitude extraction from a single defocused image of a homogeneous object. J Microsc 2002;206:33–40.
[37] Brun F, Massimi L, Fratini M, Dreossi D, Billé F, Accardo A, et al. SYRMEP Tomo Project: a graphical user interface for customizing CT reconstruction workflows. Adv Struct Chem Imag 2017;3:4.
[38] Freeman WT, Adelson EH. The design and use of steerable filters. IEEE Trans Pattern Anal Mach Intell 1991:891–906.
[39] Kumar AT, Chung E, Raymond SB, van de Water JA, Shah K, Fukumura D, et al. Feasibility of in vivo imaging of fluorescent proteins using lifetime contrast. Optics letters. 2009;34:2066-8.
[40] Schneider CA, Rasband WS, Eliceiri KW. NIH Image to ImageJ: 25 years of image analysis. Nat Methods 2012;9:671.
[41] Gonzalez-Tendero A, Zhang C, Balicevic V, Cárdenes R, Loncaric S, Butakoff C, et al. Eur Heart J Cardiovasc. Imaging. 2017;18:732–41.